The mechanical basis of impaired esophageal emptying postfundoplication

Sudip K. Ghosh, Peter J. Kahrilas, Tamer Zaki, John E. Pandolfino, Raymond J. Joehl and James G. Brasseur

AJP - GI 289:21-35, 2005. First published Feb 3, 2005; doi:10.1152/ajpgi.00235.2004

Am J Physiol Gastrointest Liver Physiol 289: G21–G35, 2005.
First published February 3, 2005; doi:10.1152/ajpgi.00235.2004.

The mechanical basis of impaired esophageal emptying postfundoplication

Sudip K. Ghosh,[1] Peter J. Kahrilas,[2] Tamer Zaki,[1] John E. Pandolfino,[2] Raymond J. Joehl,[2,3] and James G. Brasseur[1]

[1]*Department of Mechanical Engineering, The Pennsylvania State University, University Park, Pennsylvania; Departments of* [2]*Medicine and* [3]*Surgery, Northwestern University's Feinberg School of Medicine, Chicago, Illinois*

Submitted 26 May 2004; accepted in final form 26 January 2005

Ghosh, Sudip K., Peter J. Kahrilas, Tamer Zaki, John E. Pandolfino, Raymond J. Joehl, and James G. Brasseur. The mechanical basis of impaired esophageal emptying postfundoplication. *Am J Physiol Gastrointest Liver Physiol* 289: G21–G35, 2005. First published February 3, 2005; doi:10.1152/ajpgi.00235.2004.—Fundoplication (FP) efficacy is a trade-off between protection against reflux and postoperative dysphagia from the surgically altered mechanical balance within the esophagogastric segment. The purpose of the study was to contrast quantitatively the mechanical balance between normal and post-FP esophageal emptying. Physiological data were combined with mathematical models based on the laws of mechanics. Seven normal controls (NC) and seven post-FP patients underwent concurrent manometry and fluoroscopy. Temporal changes in geometry of the distal bolus cavity and hiatal canal, and cavity-driving pressure were quantified during emptying. Mathematical models were developed to couple cavity pressure to hiatal geometry and esophageal emptying and to determine cavity muscle tone. We found that the average length of the hiatal canal post-FP was twice that of NC; reduction of hiatal radius was not significant. All esophageal emptying events post-FP were incomplete (51% retention); there was no significant difference in the period of emptying between NC and post-FP, and average emptying rates were 40% lower post-FP. The model predicted three distinct phases during esophageal emptying: hiatal opening (*phase I*), a quasi-steady period (*phase II*), and final emptying (*phase III*). A rapid increase in muscle tone and driving pressure forced normal hiatal opening. Post-FP there was a severe impairment of cavity muscle tone causing deficient hiatal opening and flow and bolus retention. We conclude that impaired esophageal emptying post-FP follows from the inability of distal esophageal muscle to generate necessary tone rapidly. Immobilization of the intrinsic sphincter by the surgical procedure may contribute to this deficiency, impaired emptying, and possibly, dysphagia.

lower esophageal sphincter; gastroesophageal reflux disease; dysphagia; mathematical model; tone

NORMAL PHYSIOLOGY of the esophagogastric segment (EGS) underlies dual mechanical functions: *1*) to allow effective passage of material antegrade and retrograde at appropriate times during a swallow, belch, or regurgitation, and *2*) to resist reflux of gastric content at inappropriate times and prevent excessive gastroesophageal reflux. The biomechanical parameters that drive opening and flow across the EGS are directly related to the physiological interactions that alter active muscle fiber tension, to resting state geometry, and to stiffness of the esophageal wall and surrounding structures. That reflux is a common occurrence in the healthy esophagus attests to the complexity of the interplay between mechanics and physiology underlying the dual functions of the EGS (15), a complexity that fundoplication (FP) attempts to reestablish surgically for sphincteric segments that fail to guard adequately against chronic reflux (7).

However, enhancement of the mechanical barrier to reflux with a FP wrap also increases resistance to esophageal emptying during a swallow. It is therefore not surprising that postoperative dysphagia is a complication of FP (1, 2, 12, 22) and that the frequency and severity of this complication depends on the details of the surgical procedure (14). Postoperative dysphagia is related to the alterations in the mechanical relationships among muscle tension, bolus flow, and luminal geometry associated with the FP. The overall objective of this study is to quantify these mechanical relationships in normal esophageal emptying and to determine the mechanical alterations that underlie postoperative dysphagia.

The emptying phase of esophageal bolus transport is marked by the formation of a distal esophageal bolus cavity (or "distal cavity") during a period when circular muscle contraction drives the bolus tail into the distal esophagus against high (or infinite) resistance at the hiatus, forcing the lumen to distend and assume a bulbous shape as bolus fluid accumulates within a shortening segment. In the normal esophagus, the distal cavity evolves into a phrenic ampulla (6) as bolus tail velocity slows to <1 cm/s and the sqaumocolumnar junction (SCJ) is pulled orad 2–3 cm over the cavity surface (21) by longitudinal muscle shortening within the esophageal body (8, 11, 26, 34). Experiments in which abdominal pressure was increased with a cuff demonstrated that cavity pressure adjusts to the intragastric pressure before the hiatus opens and esophageal emptying begins (9, 32). More recent manometry studies suggest that pressurization of the distal cavity precedes hiatal opening and initiates transhiatal flow, both in the normal esophagus and in the presence of hiatal hernia and FP (16, 21). Delineation of the physiological mechanics underlying distal bolus cavity pressurization and the mechanical disruptions associated with impaired esophageal emptying underlie a clear understanding of the requirements for the minimization of dysphagia following surgical restoration of the EGS.

Specific objectives of this study were therefore *1*) to delineate the mechanical relationships among distal cavity "driving pressure" and cavity muscle tone required to open the sphincteric segment and force bolus fluid across a hiatal canal against high frictional resistance, the time history of hiatal canal opening, and the rate of esophageal emptying across the normal EGS; *2*) to quantify the mechanical relationships underlying impaired esophageal emptying post-FP; and *3*) to examine surgically controllable parameters of the FP wrap in context with the mechanics of esophageal emptying to suggest

Address for reprint requests and other correspondence: J. G. Brasseur, Professor of Mechanical and Bio Engineering, 205 Reber Bldg., The Pennsylvania State Univ., University Park, PA 16802 (e-mail: brasseur@psu.edu).

The costs of publication of this article were defrayed in part by the payment of page charges. The article must therefore be hereby marked "*advertisement*" in accordance with 18 U.S.C. Section 1734 solely to indicate this fact.

surgical adjustments to reduce impaired postoperative dysphagia. Our analysis combines concurrent manometric pressure and fluoroscopic imaging data with mathematical models to quantify flow rate and evaluate effects of varying surgical parameters. To quantify the active muscle tone that generates the driving pressure within distal bolus cavity, we combine our measurements of distal cavity pressure with a Newton's law force balance of the muscle wall. It is through the combination of physiological data with the laws of mechanics in mathematical form that we determine the normal pressure-flow-geometry relationships and the alterations underlying impaired emptying post-FP.

MATERIALS AND METHODS

Physiological data collection. Concurrent manometry and videofluoroscopy data were collected from seven healthy normal controls (NC) (3 women and 4 men) between the ages of 26 and 43 yr (mean age, 34 yr), and seven post-FP (FP) patients (1 man and 6 women) between the ages of 42 and 66 yr (mean age, 54 yr). Subjects for the study were derived from a pool of normal volunteers and patients previously diagnosed with symptomatic reflux disease who had undergone laparoscopic Nissen FP. None of the post-FP patients had evidence of Barrett's epithelium on the basis of prior endoscopy. The normal subjects had no known symptoms of reflux (heartburn, dysphagia, regurgitation, chest pain) and no known history of any anatomic defects such as hiatus hernia. All subjects gave informed written consent to the study, which was approved by the Northwestern University Institutional Review Board and conformed to the Declaration of Helsinki standards.

All laparoscopic Nissen FPs were performed by the same surgeon (R. J. Joehl). Versed (midazolam) 1 to 5 mg and fentanyl 0 to 100 mcg were used for anesthesia. The technique of laparoscopic Nissen FP included these elements: *1*) at least 10 cm of the proximal gastric fundus was mobilized by dividing the short gastric vessels; *2*) retroperitoneum over the left medial aspect of the diaphragmatic crux was incised reducing the hiatus hernia; *3*) proximal lesser gastric curvature and esophagogastric junction (EGJ) were dissected, incising the gastrohepatic omentum, which exposed the right half of the diaphragmatic crux and opened the retroesophageal space; *4*) EGJ was surrounded with a one-half-inch latex rubber drain for retraction; *5*) a 50-Fr Maloney dilator was inserted through the mouth across the EGJ; *6*) the dilated hiatal opening was narrowed by one or two nonabsorbable sutures, approximating the right and left bundles of the crux behind the esophagus; *7*) the gastric fundus was pulled through the retroesophageal opening, and the fundic wrap was secured with two or three interrupted nonabsorbable sutures, each placed 1 cm apart, anchoring the proximal sutures to esophageal musculature above the anatomic EGJ; *8*) thus the wrap was roughly 3 cm in length. All patients reported a period of postoperative dysphagia, requiring caution while eating solid food for a period of about 6 wk. However, by the time of the study, 6 mo postprocedure, all were on an unrestricted diet, reporting only rare instances of difficulty in swallowing solid food, and were taking no antisecretory medication. Further details are given in Tatum et al. (36).

In all NC and post-FP patients, a single swallow of a 10-ml bolus of standard liquid barium (Liquid E-Z; E-Z EM, Westbury, NY), selected from the middle of the study to allow subjects to adapt to the procedure, was evaluated. When esophageal emptying was incomplete, only the first peristaltic sequence was quantified. Concurrent manometry and videofluoroscopy were carried out with the individual in a supine position. Subjects were positioned supine beneath a C-arm fluoroscope and exposed to radiation at a rate of 1 Rad/min with total exposure time limited to a maximum of 5 min. Total exposure was <5 Rads, which is less than that encountered in a typical clinical gastrointestinal series. Subjects were provided with pelvic and thyroid shielding.

Manometry was carried out with a 13-lumen silicone rubber manometric catheter (4.4 mm outer diameter; Dentsleeve, Bowden, South Australia) with four side holes arranged axisymmetrically in a ring to enable accurate placement of the catheter within the high-pressure zone by a pull through. Seven side holes were spaced above the ring and one below the ring at 1.5-cm intervals with radiopaque markers just distal to each side hole, and a gastric side hole measured pressure 6 cm distal to the ring. Each catheter lumen was perfused by a low-compliance perfusion pump at 0.3 ml/min (Dentsleeve Mark II; 16-channel model); rise rates were at least 200 mmHg/s. The pressure transducers were connected to a computer polygraph and sampled at 40 Hz (Neomedix Systems, Warriewood, NSW, Australia) using the Neomedix Gastromac software. Manometric tracings and fluoroscopic images were synchronized using a video timer (model VC 436; Thalner Electronics Laboratories, Ann Arbor, MI), which encoded time in hundredths of a second on each video frame and sent a 1-V 10-ms pulse to an instrumentation channel of the polygraph at whole-second intervals. The subject breathed normally during the swallow.

Physiological data analysis. The VHS video images were digitized at 10 frames/s using a SGI Indigo 4000 computer (Silicon Graphics, Mountain View, CA) equipped with a frame-grabber, and an editing video cassette recorder (Panasonic model 7500A). Digitized images were subsequently quantified in coordination with manometric pressure using an in-house image processing system developed within the Matlab software environment (version 6.5; The Mathworks, Natick, MA). Geometric parameters were extracted from the images over the period of time from the opening of the hiatus to either the time of hiatal closing (NC) or to the time of the first retrograde flow event (post-FP). The geometric parameters measured are shown in Fig. 1

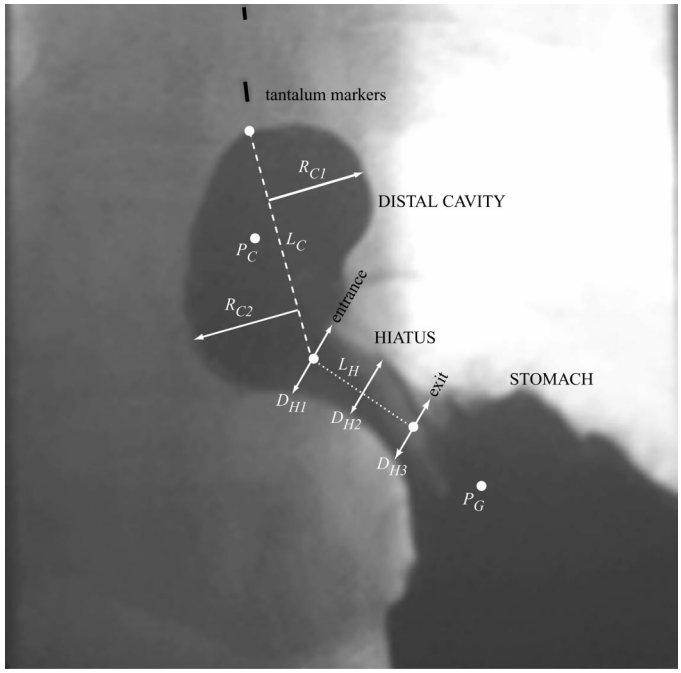

Fig. 1. Videofluoroscopic image of emptying of a radiopaque bolus across the esophagogastric segment (EGS). Videofluoroscopic images were digitized at each time instant during esophageal emptying and the following measured geometrical parameters: length of distal bolus cavity (L_C), radius of cavity measured at two locations on either side of the bolus axis and averaged (R_C), length of hiatus (L_H), and diameter of hiatus at three locations along the hiatal length and averaged (D_H). The separation between tantalum markers was used to calibrate distances in physical units. Cavity pressure (P_C) measured at the midpoint of the distal bolus cavity and gastric pressure (P_G) were recorded from manometry data at each time step.

and described next. All lengths were calibrated using the known distance between tantalum markers.

The most proximal location of the distal bolus cavity (the cavity tail) was defined as the bolus/no-bolus interface along the manometric catheter at each time instant (Fig. 1). The entrance to the hiatus was defined visually as the location at which the diameter of the cavity decreased sharply, whereas the exit was defined by a rapid increase in bolus diameter from a relatively straight hiatal canal. The length of the hiatus, L_H, was defined as the linear distance between the two points in the middle of the hiatal entrance and exit (Fig. 1). The diameter of the hiatus (D_H) was defined as the average of the diameters at the entrance (D_{H1}), middle (D_{H2}), and exit (D_{H3}) of the hiatus in Fig. 1. Hiatal radius $R_H = D_H/2$. The length of the distal esophageal bolus cavity (L_C), was defined as the straight-line distance from the cavity tail to the entrance of the hiatus. The shape of the distal cavity shown in Fig. 1, specifically the absence of axial symmetry, was typical of most swallows. The "radius of the cavity" (R_C) was therefore defined as the average of the two "radii" (R_{C1} and R_{C2}) defined as the maximum distances perpendicular to the line connecting the cavity head and hiatal entrance (dashed line in Fig. 1). These four parameters (L_C, R_C, L_H, and R_H) were recorded at each time instant during the esophageal emptying period. All radii presented in this paper include the radius of the manometric catheter. Cavity bolus volumes were estimated by inserting L_C, R_C, and R_H into the mathematical expressions for the cavity geometry shown in Fig. 2 and discussed in *Biomechanical analysis*. The volume occupied by the manometric catheter was not included in the calculation of bolus cavity volume. However, all radii are measured from the catheter axis.

By coordinating manometry with video, the time rate of change of pressure at the midpoint of the distal bolus cavity [cavity pressure (P_C)] was determined at the manometric sampling rate (40 Hz). Pressures were referenced to gastric pressure, determined by averaging the pressure from the gastric port during the swallow period.

Ensemble averages in time (L_C, R_C, L_H, R_H, P_C) were done by first normalizing time in each swallow from 0 to 1 during the esophageal emptying period. After averaging, the time axes were converted from zero (hiatal opening) to the average time to hiatal closing in NC or failure post-FP. Analysis of statistical significance was carried out with the "R" statistical software package (version 1.7.0) distributed by the Free Software Foundation under the GNU General Public License. The unpaired Student's *t*-test was used to determine significance between groups (NC vs. FP); comparisons with $P < 0.05$ were considered significant. All statistics are given as means ± SD.

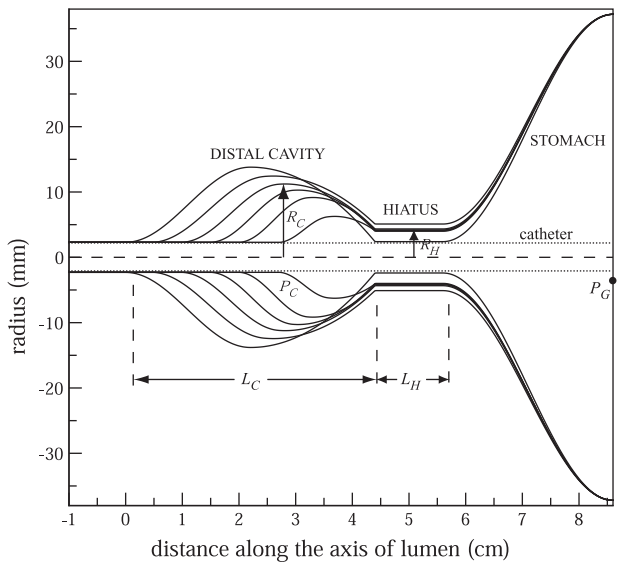

Fig. 2. The geometry model of the EGS is shown at 6 time steps during esophageal emptying. The distal bolus cavity was modeled as a bulb-like structure consisting of two different mathematical curves for the proximal and the distal halves. The hiatus was modeled as a constant diameter tube, and the gastric cardia, with a cosine curve. Temporal variations in R_C and L_C were obtained from physiological data, and P_C and P_G were specified in the mathematical models (see APPENDIX A).

Biomechanical analysis. The complex mechanical interactions that take place during hiatal opening and esophageal emptying indicate a strong biomechanical basis to the underlying physiology. Fluoroscopy and manometry are limited in their ability to quantify all important mechanophysiological variables underlying the emptying process. For example, the details of esophageal emptying rate and muscle tone driving emptying cannot be quantified in vivo with existing modalities. However, mathematical models and relationships derived from the laws of physics can be combined with physiological measurements to quantitatively extend the data to calculate biomechanical variables that are not directly measurable. We apply mathematical modeling in this study for this purpose. In this section, we give a verbal description of two biomechanical models applied in this study. The mathematical details are given in APPENDIX A.

Our mathematical models were developed from the laws of physics in combination with physiological data to quantify and explore the mechanical relationships among three primary elements of esophageal emptying mechanics: *1*) time changes in geometry of the distal bolus cavity, *2*) time changes in diameter of the hiatal canal, and *3*) the time changes in cavity pressure (reflecting muscle tone) required to drive the bolus flow against frictional resistance within the hiatus. Quantifications of transhiatal flow and esophageal emptying follow from a combination of the first two elements and determine the rate at which the liquid bolus volume enters the stomach. Because Newton's laws of mechanics govern the mechanical relationships among these three elements, it is possible, with appropriately designed mathematical models, to predict one of the three elements after specifying the other two. In this study, we develop two such models. With a "direct" model, the time-dependent geometry of the distal cavity (*element 1*) and the time history of hiatal opening (*element 2*) are specified, and the time change in cavity pressure (*element 3*) is predicted. With an "indirect" model, the time history of cavity pressure and geometry are specified and the time change in hiatal radius is predicted. Here we summarize in general terms, without mathematical detail, the primary elements of the models useful in the interpretation of results.

Design of the mathematical models requires the specification of two subelements: *1*) time-varying radius of the lumen through the distal bolus cavity, hiatal canal, and into the gastric cardia; and *2*) appropriate mathematical representation of Newton's laws of mechanics for a liquid bolus flow through the specified shape. The modeled shape of the distal cavity, hiatus, and stomach is shown in Fig. 2. The EGS is straightened in the model, and each cross section is approximated as circular. Since the physiological data include manometry, a manometric catheter is included in the model to combine and compare with the data. The time-changing distal cavity is modeled with a cosine curve over the proximal half and a quadratic curve over the distal half to meet a straight cylindrical hiatal canal with time-varying radius. All that is required of the modeled gastric cardia is that it accept bolus fluid passing from the hiatus at a diameter much higher than that of the hiatus. In the model, the time change in cavity volume (the esophageal emptying rate) is a consequence of the time changes in cavity length L_C and radius R_C together with the time change in hiatal radius R_H. To evaluate the possibility that cavity shape plays a role in pressure-flow dynamics, we carried out a series of tests in which alternative cavity shapes were used. There was no significant affect of modeled shape on predictions of cavity pressure vs. emptying rate during the emptying process.

The following approximations were made in the mathematical representation of Newton's law to model the process of bolus fluid being forced from a slowly reducing distal cavity through a hiatal canal with time-varying radius into an open gastric cardia at fixed

pressure. First, because transhiatal flow is driven by cavity pressure primarily against frictional resistance within the hiatus, pressure force is approximated as fully in balance with frictional forces, so that inertia in the flow is neglected. Second, the mathematical form of the frictional force term is simplified by neglecting axial gradients in flow velocity relative to radial gradients. This strategy has been used to great effect in modeling peristaltic transport in the esophageal body (19, 27, 25), and both approximations have been evaluated and validated for our current application (see APPENDIX A).

A "direct" model was used to predict cavity-driving pressure vs. transhiatal flow after inserting into the model a parameterized time history of average hiatal radius obtained from the physiological data. We discovered, however, that the initial opening of the hiatus displays extreme sensitivity between time variation in cavity pressure and the fine details of hiatal opening. We therefore developed a more accurate "indirect" model that predicts hiatal opening with the measured time changes in average cavity pressure as an input (APPENDIX A). The indirect model was subsequently applied to a detailed analysis of the time-dependent hiatal opening and transhiatal flow relationships. All model calculations assumed a bolus viscosity of 500 cP consistent with liquid barium sulfate boluses (20). Complete details of the model, including the mathematical developments, are given in APPENDIX A and references therein. Specific details of specific model calculations are given in RESULTS.

Calculation of muscle tone over the distal esophageal bolus cavity. Generation of tone underlies muscle contraction and fluid propulsion. "Tone" is synonymous with the mechanical "stress" generated in the muscle wall in response to "active" neurological stimulation of muscle fibers. Stress is defined as the total summation of fiber force per unit area of muscle tissue perpendicular to the fibers. Total wall stress is the summation of tone (active stress) and a "passive" stress component that arises purely in response to elastic stretch of the wall tissue with or without neurological stimulation (see Ref. 25). The muscle wall over the distal bolus cavity contains circular and longitudinal muscle fibers that generate stress in circumferential and axial directions. An increase in net muscle tone over the distal bolus cavity can increase fluid pressure that, if sufficient, can force open the hiatal canal and initiate esophageal emptying.

It is not possible to measure tone directly in vivo in humans. However, it is possible to compute tone from data, which can be measured by applying the laws of mechanics to derive mathematical relationships that relate stress to distal bolus cavity pressure and geometry, measured from concurrent manometry and fluoroscopy. Details of this mathematical development are given in APPENDIX B. Here we describe briefly the elements that enter the development and give the final mathematical equation from which tone is computed from data generated from the manofluoroscopic data sets described earlier.

The development centers on the application of Newton's law of motion to derive a mathematical relationship between total wall stress, pressure difference between the distal bolus cavity and mediastinum, geometry of the distal bolus cavity, and the thicknesses of the muscle and mucosal layers at peak bolus cavity radius. The resulting mathematical expression is rewritten in a form that involves driving pressure difference between the distal bolus cavity and stomach, measured from manometry. We separate total stress into active and passive components and develop a separate relationship between passive stress and cavity pressure using manofluoroscopic data collected in the distal esophagus in the inhibited state during peristalsis (see Ref. 25). To complete the derivation, it is necessary to know the thickness of the muscle and mucosal layers at maximum cavity radius during emptying. To determine these, we apply another fundamental law of physics, conservation of wall mass. Using this law, one can determine muscle and mucosal wall thicknesses at any measured luminal radius from knowledge of the resting state thicknesses. These have been reported in several separate studies.

As described in APPENDIX B, combining the application of Newton's law with a model for passive stress leads to a relationship among active stress (tension) (T_A) in the wall surrounding the distal bolus cavity, driving cavity pressure relative to gastric ($P_C - P_G$), cavity radius and length (R_C and L_C), and muscle thickness (t)

$$T_A \approx \frac{R'_C}{t}\left[1 + \left(\frac{2R'_C}{L_C}\right)\right]^{-1}[(P_C - P_G) - mR_C + G] \qquad (1)$$

Because T_A is defined as force per unit muscle area (as opposed to per unit length of lumen, as is sometimes done), T_A may be interpreted as average muscle fiber force. $R'_C = R_C + t_M$ is the maximum radius of the distal bolus cavity to the inner muscle boundary, where t_M is the thickness of the mucosal layers (mucosae). G is the gastric pressure relative to mediastinal pressure, which we approximate as 5 mmHg. The parameter *m* in *Eq. 1* describes the stiffness of the distal esophageal wall muscle in response to passive stretch, with passive defined as the inhibited state preceding peristalsis (25). Four sets of pressure-radius data obtained from the bolus head region during peristalsis (see APPENDIX B) indicate a roughly linear relationship between intraluminal pressure (relative to atmospheric) and luminal radius. We quantified the stiffness parameter *m* from the average of four sets of pressure-radius curves to be 11.5 mmHg/cm.

Eq. 1 is a generalization of the Laplace equation for an ellipsoidal distal bolus cavity with T_A properly interpreted as an average of circular and longitudinal muscle stresses. Before applying this equation, we must compute the muscle and mucosal layer thicknesses (t and t_M). Mathematical equations that relate layer thickness to cavity radius and resting state values are derived in APPENDIX B by stipulating that mass and volume be conserved within the muscle layer (26). Data for the resting-state thicknesses of the mucosae and muscularis (t^*_M and t*) were obtained from measurements by Ulerich et. al. (37), who measured the spatial variation of muscle wall thickness in the distal esophagus for 10 normal subjects using high-frequency ultrasonography. The mathematical expressions for thickness involve a parameter for longitudinal extension of the muscularis relative to the resting state. These data were obtained from the study of Shi et al. (34).

To test the sensitivity of our calculations to the stiffness and thickness parameters taken from the literature, we systematically varied the various parameters by ±30%. Whereas the resulting curves shifted in magnitude as much as ±30%, the shapes of the curves and the conclusions remained unchanged.

RESULTS

Basic characteristics: analysis of physiological data. The propagation speed of the bolus cavity tail was always <1 cm/s in both subject groups, identified by Lin et al. (21) as one of three criteria for the existence of a phrenic ampulla. However, the criterion that the SCJ be displaced orad 2–3 cm over the ampullary surface was not met in post-FP emptying of the distal bolus cavity (21), and an obtuse angle at the cavity tail was only sometimes observed. Every post-FP swallow failed to completely clear the bolus from the esophageal lumen in the first swallow. As summarized in Table 1, whereas the NC group achieved nearly complete clearance of bolus fluid (97.2% average), bolus clearance post-FP was only 49.2% (average) after the first swallowing attempt ($P < 0.01$). However, the transhiatal emptying period was similar for NC and post-FP subjects (3.81 ± 0.92 vs. 4.10 ± 1.26 s; $P > 0.2$) and, consequently, the average emptying rate was much lower in the post-FP group (3.3 ± 1.3 vs. 1.98 ± 1.4 ml/s, $P < 0.05$).

The time changes in cavity length, radius, and volume of NC and post-FP are compared in Fig. 3. Whereas cavity length and

Table 1. *Overall emptying statistics*

	Emptying Time, s	R_H, mm	L_H, cm	Cavity Volume: Initial Volume, ml	Cavity Volume: Volume After First Swallow, ml	Cavity Volume: % Volume Retained	Esophageal Emptying Rate, ml/s
NC	3.81±0.92	5.03±1.12	1.21±0.20	12.8±4.81	0.32±0.19	2.81±1.20	3.28±1.31
FP	4.10±1.26	4.37±0.84	2.37±0.71	14.2±6.21	6.11±5.30	50.8±28.5	1.98±1.35
P value	>0.2	>0.2	0.000865	>0.2	0.00725	<0.01	0.047

Values are means ± SD; NC, normal controls; FP, postfundoplication; R_H, radius of hiatus (with catheter); L_H, length of hiatus.

radius decreased roughly linearly for the first 2.5–3 s of normal esophageal emptying, over the last 1–1.5 s both cavity length and radius decreased more rapidly, and, consequently, the bolus emptied completely in the NC group (Fig. 3*C*). In contrast, there was a much slower rate of decrease of volume in the post-FP group (Fig. 3*C*, Table 1), which followed from the lower rates of decrease in cavity length and radius (Fig. 3, *A* and *B*). Furthermore, rather than a speedup in the reduction of cavity length, radius, and volume toward the end of the emptying period, the rates of reduction in these quantities decreased in the post-FP group, implying bolus retention (Fig. 3*C*).

The hiatal canal was almost twice as long post-FP compared with NC (2.37 ± 0.7 vs. 1.21 ± 0.2 mm; $P < 0.001$; Table 1). There was a statistically insignificant 13% reduction in average maximum hiatal radius in the post-FP group compared with NC (4.37 vs. 5.03 mm, including catheter radius, $P > 0.2$, Table 1). As shown in Fig. 4, on average the hiatal radius in NC opened rapidly, overshot, then rebounded to a quasi-steady level for roughly 2 s before closing rapidly near the end of the esophageal emptying period. In contrast, opening in the presence of FP was initially much slower than normal, did not overshoot or rebound, and did not rapidly close at the end of the esophageal emptying period (Fig. 4).

As shown in Fig. 5, there were major differences in evolution of average cavity pressure (plotted relative to gastric pressure) during esophageal emptying between NC and post-FP subjects. Overall, the rate of increase in pressure was higher in the normal group, although average pressure during emptying was comparable. In particular, the normal rates of increase in cavity pressure were much higher during the initial (*phase I*) and final (*phase III*) periods, compared with subjects with FP. During the middle period (*phase II*), pressures were roughly the same in both groups, with cavity pressure higher in the initial period and lower in the final period in the FP group relative to normal cavity pressure.

Mechanical balance: predictions from biomechanical analysis. Figure 6 shows the results of a direct model calculation (see MATERIALS AND METHODS) designed to explore basic relationships between tightness and length of wrap, cavity pressure (reflecting muscle tone), and the rate of esophageal emptying. The parameterized geometry variations shown in Fig. 6*A* were input into the direct model as first approximations of the physiological data shown in Fig. 3. Normal was defined as $R_H = 5.03$ mm, $L_H = 1.21$ cm, and esophageal emptying period = 3.81 s (Table 1). We asked the following two questions of the direct model. If a FP wrap were to cause a decrease in hiatal radius and/or an increase in hiatal length relative to a normal hiatal canal, *1*) how might we expect average cavity pressure (and muscle tone) to change to maintain normal esophageal emptying rates, and *2*) how would the rate of emptying have to change to maintain normal levels of cavity pressure (muscle tone) during the emptying process?

The model calculations are shown in Fig. 6*B*, in which percent deviations from normal are plotted for FP hiatal length = 2.37 cm (Table 1). The solid curve shows that for the distal bolus cavity in the presence of FP to empty at the same rate as normal, the esophageal muscles surrounding the cavity would have to produce pressures 200–350% higher than normal when the FP wrap reduces the hiatal radius 20–30% from normal. To address the second question, the modeled period of emptying was systematically increased, as the hiatal radius was systematically decreased from 5 to 3.5 mm (Fig. 6*A*) to produce the same average cavity pressure as normal. The result (Fig. 6*B*, dashed curve) indicates that reductions in average flow rate of order 200–300% would be required to empty the distal cavity with normal levels of cavity pressure (and tone). The effect of a lengthened hiatus is given by %decrease in radius of wrap at zero. The model suggests that a 50–60% change in esophageal emptying rate or pressure is required to overcome the added resistance by an extended hiatal canal length from the FP wrap.

Whereas the direct model was useful to predict the general behaviors in Fig. 6, it also predicted very high sensitivity between the details of hiatal opening and cavity pressure during opening, resulting in an inaccurate representation of the pressure-flow dynamics during the opening period. To overcome this difficulty, we applied the indirect model described in MATERIALS AND METHODS, which accurately predicted the opening period. Smoothed versions of the time changes in average cavity radius, length, and pressure (Figs. 3 and 5) were inserted into the model (see APPENDIX A), and the time changes in average hiatal radius were predicted. The predictions, shown in Fig. 7, were in very good qualitative and quantitative agreement with the measured hiatal radius in both the NC and post-FP groups. The mathematical model predicted the overshoot in hiatal radius during normal opening at about 0.75 s, as well as the absence of an overshoot in the post-FP patient group. Other qualitative details well predicted included a much higher rate of opening of hiatal radius in NC compared with FP, a momentary decrease and increase in hiatal radius in NC at 2.0 to 2.4 s, and a sudden reduction in hiatal radius in the post-FP group at about 2 s. The model predictions of maximum hiatal radius were about the same for NC and post-FP, statistically consistent with measurement and within the standard deviations of the data.

Figure 8 compares the time variations in esophageal emptying rate of NC and post-FP subjects calculated from the

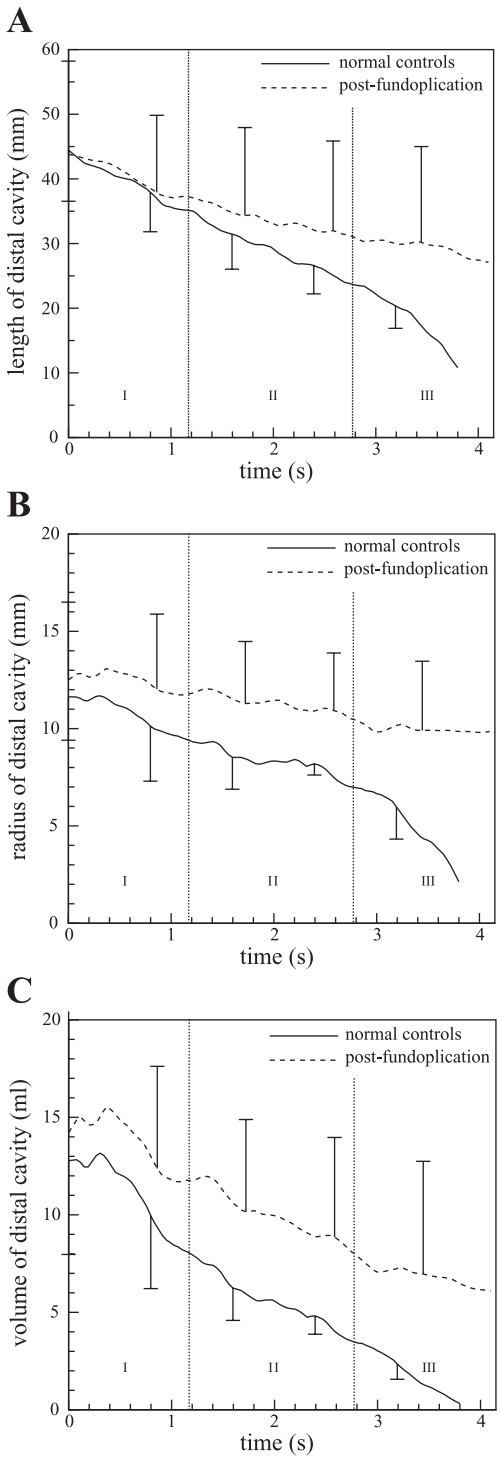

Fig. 3. Temporal variations in average length (*A*) and average radius (*B*) of the distal bolus cavity measured for normal controls (NC; solid line) and postfundoplication (post-FP subjects; dashed line). The time variation in average cavity volume is shown in *C*, using the geometrical model (Fig. 2) to calculate volume from R_C and L_C at each time for each subject. All average parameters were calculated by first normalizing the esophageal emptying time for each swallow from 0 to 1 and, once averaged, multiplying the normalized times by the average emptying time in each group (Table 1). Bars indicate standard deviations (7 subjects per group). Vertical dotted lines demarcate *phases I*, *II*, and *III* (see phases of esophageal emptying discussion above Fig. 5).

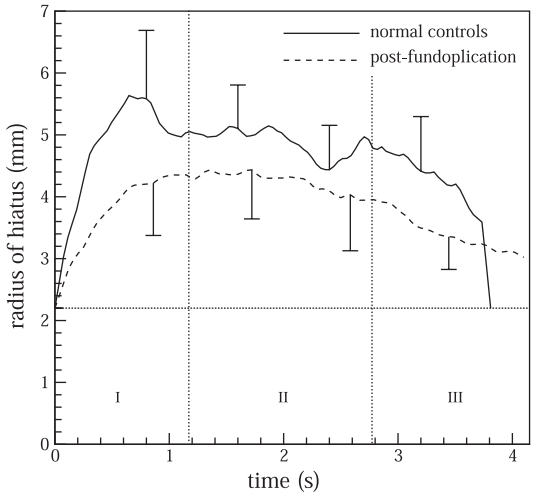

Fig. 4. Temporal variations in hiatal radius for NC (solid line) and post-FP (dashed line) groups are shown. The dotted line at 2.2 mm shows the radius of the catheter. The average hiatal radius was calculated from each individual swallow as explained in Fig. 3. Bars indicate SDs (7 subjects per group). The vertical dotted lines demarcate *phases I*, *II*, and *III*.

indirect mathematical model with physiological data inputs. Three phases to esophageal emptying were predicted. During the initial opening period (*phase I*), the esophageal emptying rate in NC increased rapidly to a peak before dropping rapidly to a rough plateau in *phase II*. In contrast, the post-FP emptying rate during *phase I* was much reduced from the NC, increasing only gradually to a plateau in *phase II*. The middle *phase II* period was characterized by a roughly constant esophageal emptying rate comparable between the NC and post-FP groups. During the final closing period, *phase III*, the emptying rates were lower than *phase I*, but again the emptying rates for post-FP patients were much lower than NC subjects. Whereas in the NC group the *phase II* and *phase III* emptying rates are comparable, in the post-FP group the emptying rate in *phase III* was lower than *phase II* and comparable to *phase I*.

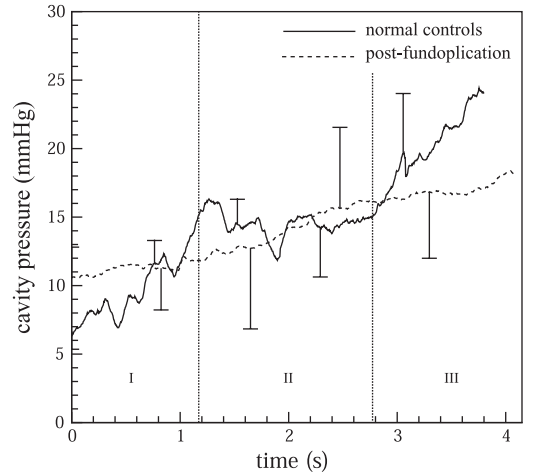

Fig. 5. Temporal variations in average cavity driving pressure referenced to gastric baseline pressure for NC (solid line) and post-FP (dashed line) groups. Averages were calculated from each individual swallow as explained in Fig. 3. The bars indicate SDs (7 subjects per group). The vertical dotted lines demarcate *phases I*, *II*, and *III*.

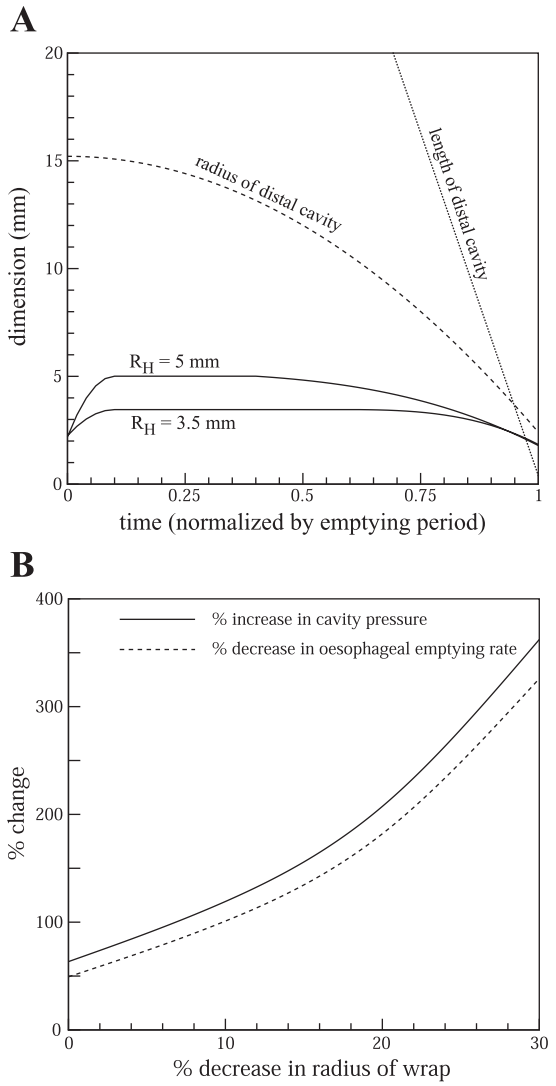

Fig. 6. Model calculations of overall sensitivities. *A*: geometrical input parameters. Tightness of wrap was varied between R_H = 5.0 mm (normal tightness) and R_H = 3.50 mm. Time change in cavity radius was approximated with a parabolic curve; cavity length was taken to decrease linearly. *B*: solid curve shows the sensitivity between hiatal radius and cavity driving pressure with average esophageal emptying rate fixed as for NC (R_H = 5.0 mm; L_H = 1.21 mm; emptying time = 3.81 s). Dashed curve line shows sensitivity of esophageal emptying rate to wrap tightness for fixed average cavity pressure. Hiatal length was 2.37 cm in both calculations.

Phases of esophageal emptying and analysis of physiological data. The demarcations of *phases I* vs. *II* vs. *III* in Fig. 8 were decided from the three periods of cavity pressure in Fig. 5 for NC. These three phases were also identifiable at about the same locations post-FP as in NC (Fig. 5), even with the more gradual increases in cavity pressure. More roughly, these boundaries also demarcated three time periods in hiatal radius (Fig. 4) and the radius, length, and volume of the distal bolus cavity (Fig. 3).

The physiological data analysis in Table 2 shows that, whereas esophageal emptying was evenly distributed between *phases I* and *II* in NC subjects (38 vs. 36%), in post-FP patients, the bulk of esophageal emptying occurred during *phase II* (48%). Both subject groups had emptied most of the final bolus volume by the end of *phase II* (75% in NC vs. 78% post-FP). However, the percent of initial volume emptied by the end of *phase II* was much less post-FP compared with NC (45 vs. 73%). The primary difference in total emptying was a result of much reduced average emptying rates (change in volume over the time period) during *phases I* and *III*. During *phase I* the average esophageal emptying rate was 40% lower in the post-FP group (2.44 vs. 4.07 ml/s), whereas during *phase III* the post-FP group emptied at a rate 57% subnormal (1.35 vs. 3.10 ml/s). These reductions in emptying rate are reflected in the total volume emptied during *phases I* and *III* combined (4.2 ml post-FP vs. 7.92 ml for NC). In contrast, the measured average rates of emptying and volume emptied during *phase II* were comparable between the NC and post-FP groups.

Muscle tone over the distal bolus cavity during esophageal emptying. Underlying the increase in cavity pressure driving hiatal opening and transhiatal bolus transport is the generation of muscle tone, or active stress, in the muscularis surrounding

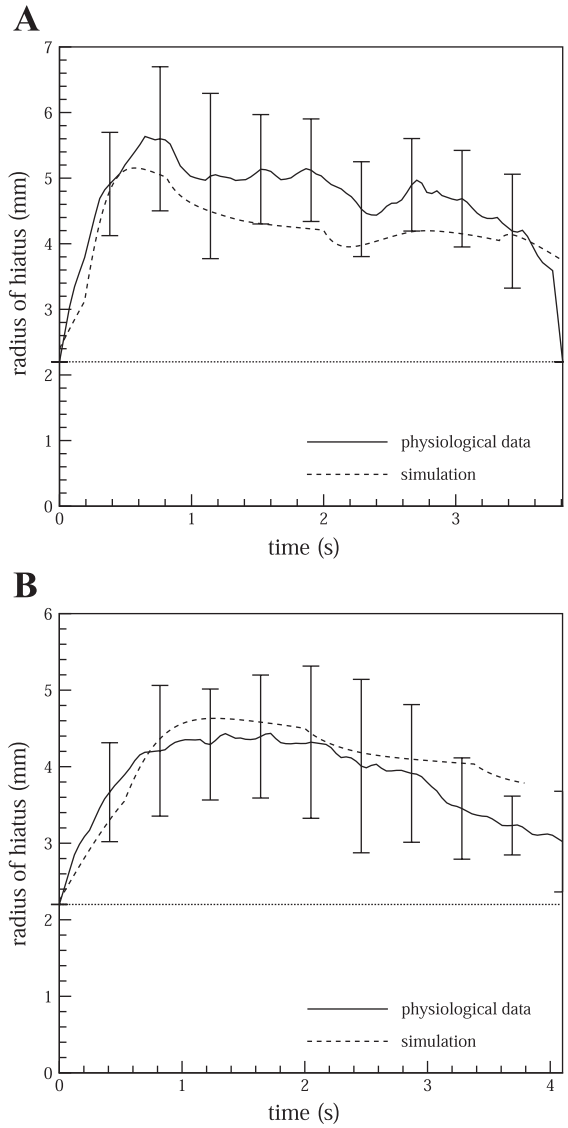

Fig. 7. Predictions of hiatal radius (dashed lines) from the indirect mathematical model are compared with physiological data (solid lines) for NC (*A*) and post-FP (*B*). Vertical bars show SD in the physiological data. Horizontal dotted lines identify the catheter radius (2.2 mm).

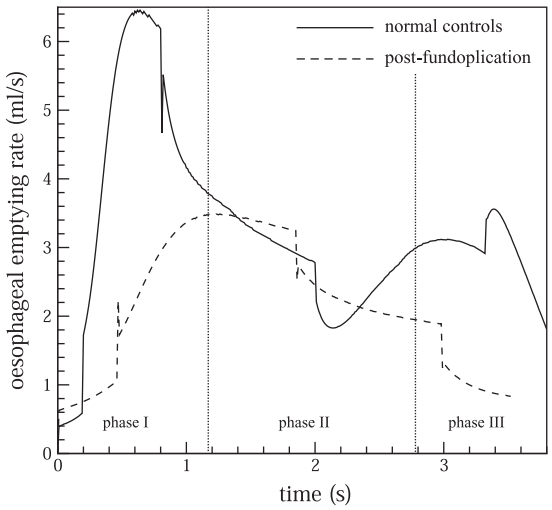

Fig. 8. Temporal variation in esophageal emptying rate is shown for NC (solid line) and post-FP (dashed line) subject groups predicted from the indirect mathematical model, with time changes in cavity driving pressure, cavity radius, cavity length input, and hiatal radius predicted (APPENDIX A). Esophageal emptying rate was calculated from the temporal changes in the cavity volume. The vertical dotted lines demarcate *phases I*, *II*, and *III*.

the distal bolus cavity. We described in MATERIALS AND METHODS and APPENDIX B the development of a mathematical model for the prediction of muscle tone (active stress) from cavity driving pressure (Fig. 5) and geometry (Fig. 3). Figure 9 shows that in normal emptying, cavity muscle tone increased rapidly, driving a rapid increase in cavity pressure (Fig. 5) and hiatal opening (Fig. 4). Active muscle stress overshot at the end of the *phase I* period before reaching a rough plateau (or decreasing slightly) during *phase II*. In contrast, cavity muscle tone in the post-FP patients increased very slowly through *phase I* and most of *phase II*, driving the slow increase in cavity pressure (Fig. 5) and slow hiatal opening (Fig. 4). As the remaining few milliliters of bolus were forced from the distal cavity in the normal *phase III* emptying period, muscle tone decreased to roughly 40 mmHg even as cavity pressure increased (Fig. 5). In the post-FP group, on the other hand, muscle tone leveled to a plateau toward the end of *phase II* and remained there through *phase III* along with cavity pressure (Fig. 5), leading to only slight reductions in cavity bolus volume, and bolus retention (Fig. 3*C*).

Table 2. *Phasic emptying statistics*

	Esophageal Emptying Rate, ml/s	Volume, ml	%Initial Volume Emptied	%Final Volume Emptied
		Normal Controls		
Phase I	4.07	4.76	37.3	38.2
Phase II	2.82	4.54	35.5	36.4
Phase III	3.10	3.16	24.7	25.4
Total		12.5	97.5	100
		Postfundoplication		
Phase I	2.44	2.44	17.2	30.1
Phase II	2.17	3.91	27.5	48.2
Phase III	1.35	1.76	12.4	21.7
Total		8.11	57.1	100

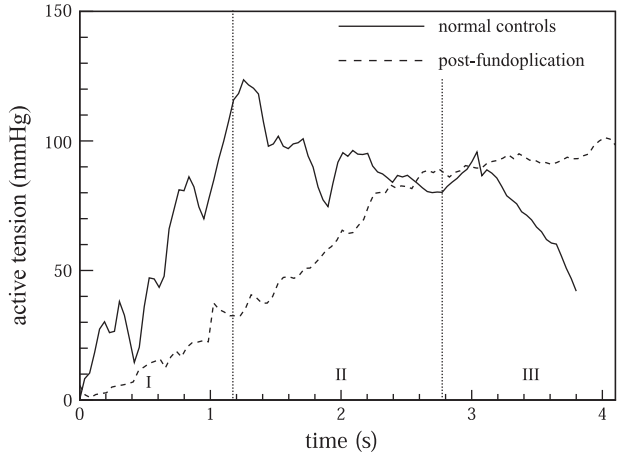

Fig. 9. Tone generation in the muscularis surrounding the distal bolus cavity during hiatal opening and esophageal emptying. Active muscle stress [active tension (T_A)] was calculated over the hiatal opening and esophageal emptying periods for the NC and post-FP groups. The function (G) in *Eq. 1* was chosen to be 7 mmHg for NC and 4 mmHg for post-FP so that the initial stress began within 10 mmHg from the time of hiatal opening.

Analysis of FP wrap parameters. Using the indirect mathematical model, computer experiments were carried out to quantify the consequences of systematic variations in tightness and length of wrap on the effectiveness of esophageal emptying post-FP. Overall esophageal emptying rates were calculated *1*) for systematic increases in maximum hiatal opening radius from the post-FP value with fixed FP hiatal length (2.37 cm, Table 1), and *2*) for systematic decreases in hiatal length from the FP value with fixed FP hiatal radius (4.37 mm, Table 1). The model predicted that only a 6% increase in hiatal radius from the average measured wrap radius (with wrap length held constant at 2.37 cm) would lead to a 50% increase in emptying rate (with the same post-FP cavity pressure), suggesting a high sensitivity between esophageal emptying rate and change in hiatal radius. Thus assuming that the period of emptying is fixed at the average post-FP value of 4.10 s (Table 1), the consequent volume of retained bolus would be reduced from 43% to roughly 13% of the initial volume. Computer experiments of variations in the length of the FP wrap showed that a lower, albeit significant, sensitivity exists between bolus retention and hiatal length. A 30% reduction in wrap length (from 2.37 to 1.66 cm) increases the esophageal emptying rate by over 50% and reduces bolus volume retention to only 14%.

We used the mathematical model to study the phase period dependency of the esophageal emptying rate on FP wrap tightness and length. It was found that the sensitivities to either increases in hiatal radius, or to decreases in hiatal length, were highest in *phase I* and lowest in *phase III*, and that the sensitivities to increasing hiatal radius were greater than to decreasing hiatal length in all phases. Furthermore, we calculated the relative sensitivity during each phase, defined as the ratio of the sensitivities in each period to the overall sensitivity. The *phase I* period was found to be relatively more sensitive to reductions in hiatal length than to increases in hiatal diameter, whereas the opposite was true during *phase III*.

DISCUSSION

The EGS is a complex physiologically controlled mechanical structure involving internal and external sphincteric com-

ponents, the interaction between circular and longitudinal muscle contraction (34), and the elastic stretch of attached membranes (3), any of which can deteriorate in myriad ways (35) leading to chronic reflux of gastric content. Combining concurrent manometric and fluoroscopic data of intraluminal pressure and geometry from NC and post-FP patients with computer models, we determine the normal mechanical relationships between driving pressure and muscle tone of the distal esophageal bolus cavity, and hiatal opening and transhiatal flow, and we evaluate the mechanical deficiencies underlying impaired esophageal emptying post-FP. We further applied the mathematical model to investigate potentially beneficial alterations to the surgical procedure to reduce resistance to emptying.

EGS function during swallowing is determined by the complex mechanical interactions among: *1*) pressure generated in the distal esophageal cavity by muscle tone over the cavity surface, *2*) resistance of the lumen to hiatal opening and maintenance of opening during flow, and *3*) frictional resistance to flow through the constricted hiatal canal. Mechanically, the force driving esophageal emptying results from the pressure difference between cavity pressure P_C and gastric pressure P_G during the period of hiatal opening, described in more detail in APPENDIX C. For example, in Fig. C1 we plot from the indirect model intraluminal pressure axially from the bolus cavity tail to the cardia at different times in the normal esophageal emptying process, relative to gastric reference pressure. Pressure within the main body of the cavity is nearly uniform and drops rapidly across the hiatal canal in response to frictional resistance. At peak hiatal radius, the pressure drop across the hiatal canal (ΔP) is approximately proportional to the volumetric rate of bolus flow into the stomach (Q), the length of the hiatal canal (L_H) and bolus viscosity (V), and is inversely proportional to average hiatal radius (R_H) to the fourth power: $\Delta P \propto V Q L_H / R_H^4$ (18). As is clear from Fig. C1, whereas the cavity-gastric pressure difference $P_C - P_G$ does not equal the transhiatal pressure drop, ΔP provides most of the contribution to $P_C - P_G$. Because gastric pressure is nearly constant during esophageal emptying, we draw the following two conclusions. First, if esophageal emptying rate (Q) were fixed, the driving pressure P_C would be very sensitive to hiatal radius (note the power 4 on R_H), and somewhat less sensitive to hiatal length and bolus viscosity (power 1 on L_H and V). Second, if the cavity driving pressure were fixed, reductions in the esophageal emptying rate will be very sensitive to reductions in hiatal diameter and somewhat less sensitive to increases in hiatal length.

These basic sensitivities are shown in Fig. 6, from which we conclude that the existence of a hiatal canal constricted by the FP wrap to subnormal diameters and lengthened to supernormal lengths requires one of two significant alterations to normal physiology: either the muscles surrounding the distal bolus cavity must generate much higher cavity driving pressure than normal to empty at normal rates, or if cavity driving pressure is limited to normal or subnormal values by limitations in muscle fiber tone, there must be major reductions in the rate of esophageal emptying, increasing the potential for bolus retention. Our physiological data indicate that it is the latter adjustment that exists post-FP; the average rate of emptying was reduced by 40% in the post-FP group (Table 1, $P < 0.05$), whereas the cavity driving pressure averaged over the time period of emptying is roughly the same for NC and post-FP patients (Fig. 5).

Interestingly, it appears that the muscles of the distal esophagus generate tone for roughly the same period of time independently of the existence of normal or altered EGS physiology (3.81 s normal vs. 4.10 s post-FP, $P > 0.2$, Table 1). The apparent existence of a "time-out" process, whereby esophageal circular muscle fibers can generate significant tone for only a fixed period of time, combined with the inability of the muscles of the distal esophagus to generate higher than normal driving pressure, has the consequence that increases in frictional resistance to flow through the hiatus due to a FP wrap necessarily leads to incomplete esophageal emptying.

The differences in tone generation between normal hiatal function and that of post-FP are dramatic, as illustrated by Fig. 9. Particularly startling is the large deficiency in the generation of cavity muscle tone post-FP during hiatal opening. Normal hiatal opening is driven by rapid generation of muscle tone of order 100 mmHg/s (Fig. 9) that in turn creates a rise in cavity pressure of order 10 mmHg/s (Fig. 5), sufficient to "blow" open the hiatus to its maximum diameter within a half second at a rate of about 9 cm/s. However, the muscles surrounding the distal bolus cavity in the post-FP group produce only 30 mmHg/s muscle tone generation (Fig. 9), less than a third the normal rate. Consequently, a very slow increase in cavity driving pressure of only 1 mmHg/s (Fig. 5) is generated, 1/10 the normal rate, with consequently slower hiatal opening at about one-third the normal rate.

The deficiency in generation of muscle tone post-FP persists through most of *phase II* (Fig. 9). Normal cavity muscle tone, in contrast, reaches a plateau during the middle period of transhiatal flow after a momentary overshoot at the transition between the *phase I* and *phase II* periods, a point in time when the hiatus has reached its maximum radius (Fig. 4). The overshoot in the model prediction of hiatal opening (Fig. 7) matches the physiological data very well and coincides with a surge of bolus flow through the hiatus (Fig. 8). This suggests that the rapid generation of cavity muscle tone creates a rapid increase in cavity driving pressure that rapidly opens the hiatus and drives a plug of bolus fluid through the hiatal canal, momentarily overstretching the hiatal lumen. No such surge exists during hiatal opening in the presence of FP (Fig. 8); the hiatus opens gradually with no suggestion of an overshoot in luminal radius (Fig. 7). We conclude that a primary distinction between the normal and post-FP opening process is the inability of the muscles surrounding the distal bolus cavity post-FP to generate the rapid increases in muscle tone required for normal opening of the EGS.

The question then arises as to the cause of the reduced muscle tone in the post-FP group. One possibility is that reflux disease is associated with a deficient tonic capability in the distal esophagus. However, another cause is possible. The normal cavity emptying process is associated with the orad excursion of the SCJ, and therefore the intrinsic sphincter, during formation of a phrenic ampulla (6, 21). This temporary herniation of the intrinsic sphincter over the distal bolus cavity before hiatal opening places it in an optimal position to contribute to the rapid generation of the cavity muscle tone, causing the sudden hiatal opening and a burst of rapid transhiatal flow. We hypothesize, therefore, that in the normal swallow, the inhibition of intrinsic sphincter tone initiated soon

after the swallow is abolished after repositioning of the sphincter orad over the ampulla, and that this reconstituted sustained sphincteric muscle squeeze is a potentially major contributor to the sudden increase in tone shown in Fig. 9. This rapid increase in tone causes the rapid increase in the driving pressure and forces open the hiatal canal. It would follow, therefore that the lack of rapid increase in cavity muscle tone, cavity driving pressure, and hiatal radius post-FP reflects, in part, the restricted axial motion of the intrinsic sphincter by the surgical procedure (16) and therefore its consequent loss to the generation of tone over the distal bolus cavity for those patients with an otherwise normal intrinsic sphincter, e.g., hiatal hernia (17).

In fact, the changes in esophageal emptying rate (Fig. 8) distinguish *phases I*, *II*, and *III* that are defined manometrically from the time changes in average cavity driving pressure (Fig. 5); the distinctions between rates of emptying between the normal and post-FP groups in the three emptying periods define the outcomes of deficient muscle squeeze behavior post-FP. Figure 8 indicates that the rates of esophageal emptying are comparable between the normal and patient groups only during the middle quasi-steady *phase II* period. In both the opening and final phases of esophageal emptying, the post-FP group is seriously deficient in its ability to empty the distal cavity. The percent of volume emptied is only 50% of the normal value during these two periods (Table 2), accounting for most of the average 51% bolus retention in the post-FP group.

Figure 3 shows that the normal *phase III* period is characterized by a sudden rapid increase in the rates at which cavity length and radius drop, and the final ejection of the remaining 25% of the bolus from the distal cavity into the stomach (Table 2). The normal final period of emptying comes at a time when cavity volume and surface area are at a minimum (Fig. 3*C*), cavity muscle tone is decreasing (Fig. 9), and the hiatus is closing (Fig. 4) causing increasing frictional resistance to flow and a rapid increase in driving pressure (Fig. 5), all taking place during a period when normal emptying rates are comparable with the *phase II* period (Fig. 8).

Post-FP emptying, however, is very different. In the final period, cavity muscle tone has reached a plateau (Fig. 9) over a bolus cavity volume that still retains 51% of its original volume, on average (Table 1). The constant cavity muscle tone together with the comparatively large cavity surface area leads to a plateau in cavity driving pressure (Fig. 5), a sudden slowing in the rates of decrease in cavity length, radius, and volume (Fig. 3) and major bolus retention (Table 2). We conclude that the low rate of emptying in the final period post-FP is strongly influenced by the existence of major bolus retention at the end of *phase II*, and therefore that the severe deficiency in muscle tone generation over the distal cavity during the opening and middle periods is at the heart of impaired esophageal emptying post-FP and, possibly, postoperative dysphagia.

The analysis above supports a mechanophysiological explanation for consistent bolus retention post-FP due to changes in muscle tension-driven cavity pressure and resistance to transhiatal flow, together with a time-out property of esophageal muscle, whereby muscle squeeze appears to be limited to roughly 4 s. It follows that increasing frictional resistance to flow will increase the likelihood of bolus retention, and therefore dysphagia. Since FP will increase the resistance to reflux, the surgical procedure involves a delicate balance between producing enough resistance to retrograde opening and flow, and minimizing resistance to antegrade flow during a swallow so as not to cause chronic bolus retention and dysphagia. We therefore used the mathematical model to quantify the effect of FP wrap parameters (namely, tightness and length of wrap) on the level of frictional resistance during emptying.

It was observed that the tightness of the FP wrap has a stronger effect on esophageal emptying rate than the length of the wrap, suggesting that this is a critical surgical variable. However, the model also suggests that the sensitivity to wrap length is sufficient that reasonable reductions in the length of the wrap can have a major impact by significantly reducing bolus retention. For example, the model suggests that a 35% reduction from the current wrap length can reduce bolus retention to only 10%. Furthermore, a phasewise analysis of transhiatal flow showed that *phase I* is the most sensitive period to changes in tightness and length of wrap. Of further significance is the observation that during the *phase I* opening period, the emptying characteristics are more sensitive to decreases in length than to increases in tightness of wrap. We, therefore, hypothesize that reducing the length of the FP wrap may have a stronger influence on hiatal opening and bolus retention during swallowing than on gastroesophageal reflux during transient lower esophageal relaxations or transient increases in gastric pressure.

In summary, this mechanophysiological study of normal and post-FP esophageal emptying concludes that the impaired emptying observed post-FP is attributable to deficiency of muscle tone in the distal esophagus during hiatal opening and esophageal emptying. Whereas optimization of geometrical parameters of the FP (particularly wrap length) has the potential to reduce severity of bolus retention by reducing resistance to flow, the reduced axial mobility of the distal esophagus associated with the surgical intervention may contribute to the weakened state of the muscularis. It follows that modifications to the surgical technique aimed at minimizing postoperative dysphagia should not only focus on minimizing tightness and length of FP to control reflux, but also on preserving the axial mobility of the distal esophagus when longitudinal motility is otherwise in tact.

APPENDIX A

Mathematical Model Development and Solution

APPENDIX A gives details of the mathematical model for those who may wish to replicate or apply similar models. To this end, it would be helpful to review Li and Brasseur (18) and Li et al. (19) and references therein.

Derivation of mathematical models. The mathematical models for flow across the EGJ were based on the basic conservation laws of physics: conservation of mass and momentum (Newton's second law). The analysis was done in cylindrical coordinates for axisymmetric geometry, as described in MATERIALS AND METHODS.

With the no-slip boundary conditions, conservation of mass for incompressible flow through an axisymmetric lumen can be written as (18)

$$\frac{\partial Q(x,t)}{\partial x} = -2\pi R(x,t)\frac{\partial R(x,t)}{\partial t} \qquad (A1)$$

where $Q(x,t)$ is the volume flow rate and $R(x,t)$ is the radius of the lumen at distance (x) along the axis of the lumen from the cavity tail

to the gastric cardia (Fig. 2) at *time t*. Our model includes a manometric catheter of radius R_C along the axis of the modeled lumen. $Q(x,t)$ is the volumetric rate of bolus flow between the catheter R_C and the epithelial lining of the mucosa, $R(x,t)$.

Models used in the analysis are based on the Navier-Stokes equation (29) in cylindrical coordinates, reduced using the two lubrication theory approximations: *1*) the flow is sufficiently friction-dominated that inertia (i.e., fluid-particle accelerations) can be neglected, and *2*) the axial changes in tube geometry are gentle enough that axial gradients in velocity can be neglected relative to radial gradients in velocity. To assess the accuracy of the first approximation for our application, the lubrication theory model was generalized to include the primary inertial term. The maximum deviation in the predicted hiatal radius was only 3.7%, which lies well within the accuracy of the experimental data, and thus validates our first approximation. The second approximation of gentle gradients in the streamwise direction has been analyzed in detail by Dusey (10) and was found to work well for predicting pressure-flow relationships even when local curvature in contractile regions is high. The consequence of the lubrication approximations is that the local flow through each cross section at x is a Poiseuille flow in nature but with pressure constant in the radial direction and varying nonlinearly along the axis of the lumen in a manner dependent on the axial changes in lumen radius in accordance with conservation of mass, *Eq. A1* (See Ref. 18 and references therein). The predicted spatial variations in pressure through our modeled EGS are described in APPENDIX C. We are lead to the following generalization of the lubrication model

$$\frac{\partial P(x,t)}{\partial x} = -\frac{8\mu}{\pi\gamma(x,t)}Q(x,t) + I(x,t) \qquad (A2)$$

where $P(x,t)$ is pressure along the lumen, μ is bolus viscosity and $I(x,t)$ is the added inertial term. $\gamma(x,t)$ is a function that depends on the cross-sectional geometry. For a circular cross section without an inner catheter, $\gamma = R^4(x,t)$. However, in the presence of a catheter of radius R_C, γ is given by (38)

$$\gamma(x,t) = [R^4(x,t) - R_C^4] - \frac{[R^2(x,t) - R_C^2]^2}{\ln(R(x,t)/R_C)} \qquad (A3)$$

In our calculations, $R_C = 2.2$ mm. *Eq. A2* without $I(x,t)$ is the classical lubrication theory model from which the pressure variation $P(x,t)$ can be obtained through numerical integration once the time changes in lumen geometry $R(x,t)$ and a pressure boundary condition are specified. In our application, we specify gastric pressure in the cardia, P_G, so that $P(x,t)$ is automatically referenced to gastric pressure. Although the model can only make predictions within a bolus-filled lumen, as explained in Li et al. (19), it is necessary mathematically to also specify the pressure within a fictitious "lubrication layer" between the catheter and mucosa proximal to the bolus tail (x in the shaded regions in Fig. C1). We specified a uniform "lubrication layer pressure" $P_0 = 5$ mmHg above gastric and carried out extensive tests to confirm that the predictions for intraluminal pressure and transhiatal flow are insensitive to the choice for P_0.

Inserting *Eq. A1* into *Eq. A2* and integrating gives the pressure throughout the lumen

$$P(x,t) = 16\mu\int_0^x \frac{1}{\gamma(s,t)}\left(\int_0^s R(s_1,t)\frac{\partial R(s_1,t)}{\partial t}ds_1\right)ds - \frac{8\mu Q_0(t)}{\pi}\int_0^x \frac{1}{\gamma(s,t)}ds + P_0 + \int_0^x I(s,t)ds \qquad (A4)$$

where $Q_0(t)$ is given by applying *Eq. A4* at the cardia [$P(L,t) = P_G$]

$$Q_0(t) = \frac{(P_G - P_0) - 16\mu\int_0^L \frac{1}{\gamma(x,t)}\left(\int_0^x R(s,t)\frac{\partial R(s,t)}{\partial t}ds\right)dx - \int_0^L I(x,t)dx}{-\frac{8\mu}{\pi}\int_0^L \frac{1}{\gamma(x,t)}dx} \qquad (A5)$$

The cavity pressure P_C was determined by evaluating *Eq. A4* at the midpoint of the cavity. The rate of volume flow $Q(x,t)$ was obtained by integrating equation *Eq. A1*

$$Q(x,t) = 2\pi\int_0^x R(s,t)\frac{\partial R(s,t)}{dt}ds + Q_0(t), \qquad (A6)$$

where $Q_0(t)$ is obtained from *Eq. A5*.

Geometry model of the lumen. As shown in Fig. 2, the luminal geometry $R(x,t)$ from the cavity tail through the hiatal canal and into the gastric cardia was modeled with several piecewise smooth mathematical curves. The cavity was separated into distinct curves over its proximal and distal halves. The proximal half was modeled with a cosine curve as follows

$$\tilde{R}(x,t) = \tilde{R}_A(t)\left[1 - \cos\left(\frac{2\pi\tilde{x}}{L_C(t)}\right)\right] \qquad (A7)$$

where $\tilde{x} = x - x_{tail}$ is the distance from the tail of the distal bolus cavity, and $\tilde{R} = R - R_C$ is the radial deviation from the catheter. The distal half of the cavity was modeled with a second-order polynomial

$$\tilde{R}(x,t) = a\tilde{x}^2 + b\tilde{x} + c \qquad (A8)$$

where $\tilde{x} = x - x_A$ is the distance from the center of the distal cavity (i.e., x_A is at R_A) and $\tilde{R} = R - R_C$ as before. Since the cavity is in two halves, in both *Eq. A7* and *Eq. A8* $\tilde{x}$ varies from 0 to $L_C/2$. The time-dependent parameters a, b and c were obtained by matching R and $\partial R/\partial x$ at the center of the cavity where the two curves meet, and by requiring $R = R_H$ where the cavity meets the hiatus. The hiatal canal was modeled as a straight tube of circular cross section with radius R_H and length L_H. From a physical perspective, the gastric cardia need only be modeled as a smooth increase from the hiatal radius at *time t* to a fixed radius R_G much larger than R_H over a distance L_G representative of the entrance to the stomach. We chose $R_G = 3.72$ cm $\gg R_H(t)$ and $L_G = 3$ cm. Because R_H is varying in time during cavity opening and closing, the curve for the cardia must also vary in time. We used a cosine curve of the form

$$R(x,t) = [R_G - R_H(t)]\left[1 - \cos\left(\frac{\pi\tilde{x}}{L_G}\right)\right] + R_H(t) \qquad (A9)$$

where here $\tilde{x} = x - x_{hiatus}$ is the distance from junction between the hiatus and cardia.

Cavity length and radius, $L_C(t)$ and $R_C(t)$, were specified by parameterizing the physiological data for NC and post-FP patients. The radius of the hiatus $R_H(t)$ was either specified (direct model) or calculated (indirect model), as explained below.

Derivation of the inertial correction term I(x,t). To evaluate the importance of inertia, we estimated the dominant inertial term, $I(x,t)$ in *Eq. A2*, and carried out a sample cavity-emptying solution with and without the inertial term to estimate its contribution. $I(x,t)$ is obtained from the quasi-steady energy balance for incompressible isothermal fluid flow through a portion of the axisymmetric lumen of small length Δx from the position x to $x + \Delta x$ (38)

$$\frac{\Delta P}{\Delta x} + \frac{1}{2}\rho\frac{\Delta(\alpha\bar{U}^2)}{\Delta x} = -\frac{\rho\bar{U}^2}{4R_{hyd}(x,t)}f \qquad (A10)$$

where $P = P(x,t)$ is pressure, ρ is bolus fluid density and R_{hyd} is the "hydraulic radius" given for our annular flow by $[R(x,t) - R_C]$. $\Delta(\ldots)$ in the numerator of *Eq. A10* signifies the difference in $(\ldots)$ between the cross sections at $(x + \Delta x)$ and x. For example, $\Delta P = P(x + \Delta x) - P(x)$. $\bar{U}(x,t)$ is the average velocity through the cross section of the lumen at x, related to the flow rate by $\bar{U} = Q/A$, where $A(x,t) = \pi[R^2(x,t) - R_C^2]$ is the cross-sectional area, and $Q(x,t)$ is obtained from the solution of equation *Eq. A6*.

The parameter $\alpha(x,t)$, traditionally called the "kinetic energy correction factor," is strictly a function of the shape of the velocity profile and is determined from an integration of $U^3(r,t)$ over the cross section (38). For our annular friction-dominated flow, the velocity profile is well approximated by local Poiseuille flow relationship

$$U(x,r,t) = -\frac{1}{4\mu}\frac{\partial P(x,t)}{\partial x}\left\{R^2(x,t) - r^2 + [R^2(x,t) - R_C^2]\frac{\ln[R(x,t)/r]}{\ln[R_C/R(x,t)]}\right\} \qquad (A11)$$

The "friction factor" f in *Eq. A10* quantifies frictional resistance to flow at cross section x, and is well approximated for our friction-dominated annular flow by

$$f(x,t) = \frac{32\zeta}{(\rho\bar{U}R_{hyd}/\mu)} \text{ with } \zeta(x,t) = \frac{[R(x,t) - R_C]^2[R^2(x,t) - R_C^2]}{\gamma(x,t)} \qquad (A12)$$

where $\gamma(x,t)$ is given by *Eq. A3*.

Combining *Eq. A12* with *Eq. A10* and taking the limit $\Delta x \to 0$ yields

$$\frac{\partial P(x,t)}{\partial x} = -\frac{8\mu}{\pi\gamma(x,t)}Q(x,t) - \frac{1}{2}\rho\frac{d(\alpha\bar{U}^2)}{dx} \qquad (A13)$$

Comparing with *Eq. A2*, we find that the inertial correction term in *Eqs. A2* through *A6* is given by

$$I(x,t) = -\frac{1}{2}\rho\frac{d(\alpha\bar{U}^2)}{dx} \qquad (A14)$$

The inertial terms in *Eqs. A4* through *A6* can therefore be integrated directly to obtain

$$\int_0^x I(s)ds = -\frac{1}{2}\rho[\alpha(x)\bar{U}^2(x) - \alpha(0)\bar{U}^2(0)] \qquad (A15)$$

In application of the model, α varied from 1.54 at the tail of the bolus to 1.66 at the distal-most position of the gastric cardia (Fig. 2). As mentioned previously, the effect of the inertia on the simulation prediction was negligible.

Direct and indirect solution methods. $P(x,t)$ and $Q(x,t)$ were obtained by integrating the terms on the right of *Eqs. A4* through *A6* using second-order quadrature based on Simpson's rule with the solution domain (cavity, hiatus, and gastric cardia) discretized into 40,000 equal segments. Doubling the number of segments did not change the solutions. With the exception of $I(x,t)$, all variables in the integrands, $R(x,t)$, $\partial R/\partial t$, and $\gamma(x,t)$, were evaluated analytically. $\bar{U}(x,t) = Q(x,t)/A(x,t)$ in *Eq. A15* was evaluated using the solution for $Q(x,t)$ at the previous time step. The time step was halved to confirm accuracy of the solution, and an optimal time step of 0.005 s was used.

In "direct" model calculations, the geometry $R(x,t)$ was fully specified throughout the modeled EGS, and $P(x,t)$ was predicted. Figure 6*B*, for example, was obtained using the time-dependent geometric parameters given in Fig. 6*A*. During opening, however, the predicted cavity pressure $P_C(t)$ was found to be extremely sensitive to minute variations in the specified time variations in $R_H(t)$, $R_C(t)$, and $L_C(t)$, a reflection of the sensitive mechanical relationships underlying the forced opening of the EGS. We therefore changed the modeling strategy to an "indirect" approach whereby the time changes in cavity geometry $R_C(t)$ and $L_C(t)$, and pressure $P_C(t)$ were specified based on physiological data and hiatal opening history $R_H(t)$ was predicted.

Integration of *Eqs. A4* through *A6* allows for a direct prediction of $P_C(t)$ from specification of $R_H(t)$, $R_C(t)$, and $L_C(t)$. Predicting $R_H(t)$, however, by specifying $R_C(t)$, $L_C(t)$, and $P_C(t)$ is indirect because iteration is required to obtain the solution. Note that *Eq. A4* requires both $R(x,t)$ and $\partial R(x,t)/\partial t$ to obtain $P_C(t)$. The iteration method was as follows. With the exception of the first-time step, at each new time step $R_H(x,t)$ was first obtained by integrating $\partial R_H(x,t)/\partial t$ from the previous time step using second-order quadrature. The solution for $P_C(t)$ was then iterated through systematic variation of $\partial R_H(x,t)/\partial t$ using the Newton-Raphson algorithm, until the predicted value of $P_C(t)$ converged to the parameterized value of $P_C(t)$. The value of $\partial R_H(x,t)/\partial t$ at the previous time step was used for the first guess at the new time step. Convergence was achieved when the predicted $P_C(t)$ was within 0.01 mmHg of the data. The first-time step was treated slightly differently. $R_H(x,t) = R_C + \varepsilon$ was specified, with $\varepsilon \ll R_C$, but the first guess for $\partial R_H(x,t)/\partial t$ was obtained from a previous direct solution. Furthermore, at the first new time step first-order, rather than second-order, quadrature was used to obtain $R_H(x,t)$.

APPENDIX B

Development of Mathematical Relationship for Active Stress

The mathematical details of the relationships used to estimate active stress (tone) within the muscularis surrounding the distal bolus cavity during esophageal emptying are given here. Useful additional discussion is given in MATERIALS AND METHODS. This development is based on the application of Newton's law force balances and the fundamental law of mechanics called "conversation of mass."

The relationship between cavity pressure P_C and the average total stress T_C within the wall surrounding the distal cavity is given by a mechanical force balance across the wall of the distal bolus cavity, approximated as ellipsoidal, at the location of the peak cavity radius point R_C

$$T_C \approx \frac{R'_C}{t}\left[1 + \left(\frac{2R'_C}{L_C}\right)\right]^{-1}(P_C - P_0) \qquad (B1)$$

where P_0 is pressure in the mediastinum, t is the thickness of the muscularis at the location of peak cavity radius, and muscle stress is defined as muscle fiber force per unit muscle area. $R'_C = R_C + t_M$ is the radius to the inner margin of the muscle layer and t_M is the thickness of the mucosal layer. As a generalization of the Laplace equation, *Eq. B1* makes the approximation that the muscle layer thickness (t) is small compared with the cavity radius R_C. *Eq. B1* reduces to the Laplace equation for a cylindrical tube when $L_C \to \infty$, and for a sphere when $L_C = 2R_C$ [derivations for these geometries can be found in fluid mechanics textbooks (38)].

The thin wall approximation is accurate when the thickness-to-radius ratio, t/R'_C, is roughly 10% or less. We can show that this is the case during the entire emptying period post-FP and through *phase II* in NC (Fig. 3*B*). It can be shown that the approximation is within 10–20% accuracy up to $R'_C = 0.3$, a constraint met for nearly the entire *phase III* period in NC in Fig. 3*B*. In deriving *Eq. B1* we also made the assumption that the stresses in the circumferential and axial directions are comparable. Thus stress should be interpreted as average circumferential plus longitudinal stress.

Our interest is in the tone generated by the muscularis surrounding the distal bolus cavity associated with the opening of the hiatus and transhiatal flow. The total stress $T_C = T_A + T_P$ is given by the summation of active (T_A) and passive (T_P) stress, where each part separately satisfies *Eq. B1* but with cavity pressure $P_C = P_A + P_P$ replaced by P_A or P_P, respectively. Active stress $T_A = T_C - T_P$ is

therefore given by *Eq. B1* with cavity pressure P_C replaced by $P_C - P_P$. However, since we shall quantify cavity pressure relative to gastric pressure P_G, and because we shall model passive pressure relative to mediastinal pressure P_0, we write $[P_C - P_P]$ as $[(P_C - P_G) - (P_P - P_0) + (P_G - P_0)]$ so that

$$T_A \approx \frac{R'_C}{t}\left[1 + \left(\frac{2R'_C}{L_C}\right)\right]^{-1}[(P_C - P_G) - (P_P - P_0) + (P_G - P_0)] \quad (B2)$$

$(P_C - P_G)$ is quantified during esophageal emptying as described in MATERIALS AND METHODS. $(P_G - P_0)$ is a fixed value of order 5 mmHg.

The relationship between passive pressure difference $(P_P - P_0)$ and cavity radius R_C defines the compliance of the muscle wall. Following Nicosia and Brasseur (25), we define passive in the smooth muscle esophagus as the inhibited state preceding a peristaltic contraction wave, and we model $(P_P - P_0)$ vs. R_C using data taken from the head of boluses during peristaltic bolus transport. Three sets of data from three separate subjects are given by Nicosia (24) and Nicosia and Brasseur (25), and data for 26 subjects are given on a single scatter plot by Ren et al. (33). In each case $(P_P - P_0)$ increased roughly linearly with luminal radius with slopes between 11 and 12 mmHg/cm (obtained by linear regression). We therefore modeled the passive compliance of the muscularis surrounding the distal bolus cavity as

$$(P_P - P_0) = mR_C + b \quad (B3)$$

with m approximated as 11.5 mmHg/cm. The value for b quantifies the prestress esophageal wall over the distal bolus cavity (13). The passive compliance data suggests that b is within a few millimeters of mercury of zero. Thus the equation for active stress is

$$T_A \approx \frac{R'_C}{t}\left[1 + \left(\frac{2R'_C}{L_C}\right)\right]^{-1}[(P_C - P_G) - mR_C + G] \quad (B4)$$

where G is roughly 5 mmHg, give or take a few mmHg and $m = 11.5$ mmHg/cm.

To complete the model, we must determine the muscle thickness (t) as a function of the measured cavity radius (R_C). Furthermore, since the radius to the muscularis is $R'_C = R_C + I_M$, we also require the mucosal thickness (t_M) as a function of R_C. As described by Nicosia et al. (26), to develop these relationships, we relate the thicknesses relative to the resting state to the local longitudinal shortening parameter $\gamma = l/l^*$, where l is the axial length of thin slice of the muscularis relative to the length in the resting state, $l^* \cdot \gamma <$ or >1 implies that the segment has shortened or lengthened relative to the resting state. Shortening ($\gamma < 1$) can only come about from local contraction of longitudinal muscle. Lengthening ($\gamma > 1$) implies that the segment has been stretched. Let the cross-sectional area of the thin slice of muscularis be A^* in the resting state and A at other times. The volume of the muscle slice is therefore l^*A^* in the resting state and lA at other times. The law of mass conservation (38) requires that the mass of the slice (i.e., density times volume) remain constant during deformation, and because muscle is incompressible (constant density) the volume of the slice must remain unchanged between the resting state and other times, so that $lA = l^*A^*$. Therefore, $\gamma = A^*/A$.

The cross-sectional area of muscularis is $A = \pi[(R'_C + t)^2 - R_C^{12}] = \pi(2R'_C t + t^2) = A^*/\gamma$. Solving the quadratic equation given by the two right-most terms gives the thickness of the muscularis

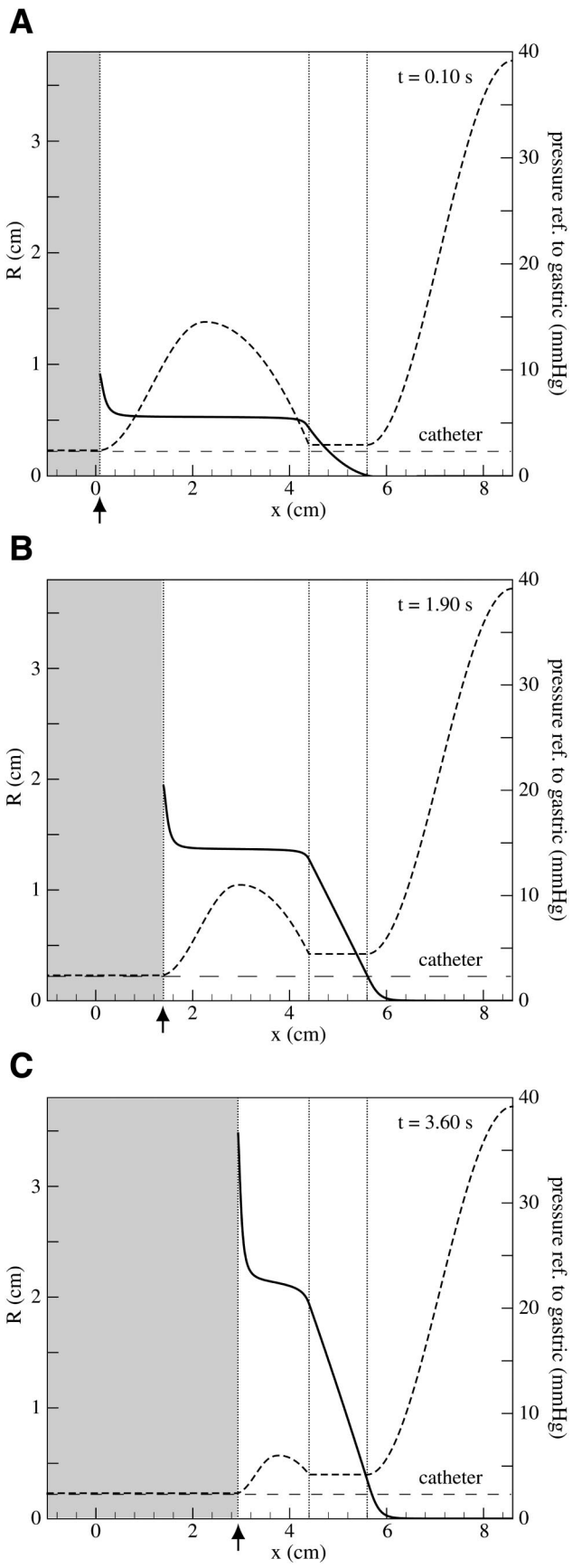

Fig. C1. Indirect model predictions of intraluminal pressure (referenced to gastric) at different times in the normal esophageal emptying process (refer to Figs. 3 and 5). *A*: hiatal opening, *phase I*. *B*: quasi-steady plateau period, *phase II*. *C*: final emptying period, *phase III*. Arrow identifies the tail, and shaded area is the contact region. R, radius; *x*, distance.

$$t = \sqrt{R_C'^2 + \frac{A^*}{\pi\gamma}} - R_C' \qquad (B5)$$

where the muscle area in the resting state is

$$A^* = \pi t^*(2R_C^* + t^*) = \pi t^*(2t_M^* + t^*) \qquad (B6)$$

Therefore, once we have a measurement of the thickness of the mucosal and muscle layers in the resting state, and once we have specified longitudinal shortening (γ), we can calculate the thickness of the muscularis at any radius R_C'. However, since $R_C' = R_C + t_M$, where R_C is the measured radius of the distal bolus cavity, we must calculate mucosal thickness t_M as a function of cavity radius R_C. To do this, we apply the same procedure as above, but to the mucosae rather than the muscularis. Assuming the same level of shortening in the mucosae and muscularis, the result is

$$t_M = \sqrt{R_C^2 + \frac{A_M^*}{\pi\gamma}} - R_C \qquad (B7)$$

where $A_M^* = \pi t_M^{*2}$.

To summarize, the procedure for determining active stress T_A in the muscularis surrounding the distal bolus cavity during hiatal opening and esophageal emptying is as follows: *1*) from the thickness of the muscle and mucosal layers in the resting state, t^* and t_M^*, determine resting state areas, A^* and A_M^*; *2*) at each measured cavity radius R_C during the transhiatal flow period, determine the thickness of the mucosae t_M from *Eq. B7*, the cavity radius to the muscularis $R_C' = R_C + t_M$, and the thickness of the muscularis (t) from *Eq. B5*; *3*) knowing cavity radii R_C and R_C', measured cavity length L_C, muscle thickness t, and the measured cavity pressure relative to gastric ($P_C - P_G$) during transhiatal flow, determine active stress from *Eq. B1*. Other details are given in MATERIALS AND METHODS.

APPENDIX C

Spatial Details of Intraluminal Pressure During Normal Esophageal Emptying

The indirect mathematical model was used to study the spatial variation of intraluminal pressure during esophageal emptying. The model predicts the entire intraluminal pressure distribution, from the tail of the cavity to the gastric cardia, from *Eq. A4*.

Figure C1 shows the predicted intraluminal pressure P (relative to gastric pressure P_G) during the normal esophageal emptying process, where $P - P_G$ is plotted with the solid curves, and lumen geometry with the dashed curves. Figure C1*A* shows the pressure distribution during the opening period (*phase I*) when cavity pressure is rapidly increasing, Fig. C1*B* shows pressure in *phase II* when $P_C(t)$ is constant and Fig. C1*C* shows pressure during the final *phase III* closing period when cavity pressure is again rapidly increasing (see Fig. 5). Intraluminal pressure is very nearly uniform throughout most of the cavity at all times, with the exception of a rapid rise near the tail and a drop at the head.

The rapid rise in pressure near the tail of the cavity is associated with a rapid rise in active muscle stress over a small portion of the bolus associated with the clamping action of a peristaltic contraction wave slowly advancing toward the hiatus, as described by Nicosia and Brasseur (25) and Li et al. (19). Proximal to the tail (the gray shaded regions in Fig. C1), the esophageal wall muscles squeeze directly onto the catheter and this contact pressure is determined entirely by the active muscle tone (4, 25).

The uniform intraluminal pressure within the cavity during emptying rises during hiatal opening and during the final emptying of the cavity, implying the existence of active muscle squeeze in the muscle wall surrounding the cavity. The difference in pressure between that at the tail of the bolus and P_C increases during opening to about 7 mmHg at the beginning of the *phase II* plateau, then decreases slowly during *phase II* before rising sharply during the final emptying phase when the pressure difference reaches 14–15 mmHg.

ACKNOWLEDGMENTS

Present addresses: Tamer Zaki, Dept. of Mechanical Engineering, Stanford University, Stanford, CA 94305; Dr. Raymond J. Joehl, Chief, Surgical Service (112) Edward Hines Jr. Veterans Affairs Hospital, 5th Ave. and Roosevelt Rd. Hines, IL 60141.

GRANTS

This research was supported by National Institute of Diabetes and Digestive and Kidney Diseases Grant R01-DK-56033.

REFERENCES

1. **Alexander HC, Hendler RS, Seymour NE, and Shires GT.** Laparoscopic treatment of gastroesophageal reflux disease. *Am Surg* 63: 434–440, 1997.
2. **Anvari M and Allen CJ.** Prospective evaluation of dysphagia before and after laparoscopic Nissen fundoplication without routine division of short gastrics. *Surg Laparosc Endosc* 6: 424–429, 1996.
3. **Bombeck CT, Dillard DH, and Nyhus LM.** Muscular anatomy of the gastroesophageal junction and role of phrenoesophageal ligament; autopsy study of the sphincter mechanism. *Ann Surg* 164: 643–654, 1966.
4. **Brasseur JG and Dodds WJ.** Interpretation of intraluminal manometric measurements in terms of swallowing mechanics. *Dysphagia* 6: 100–119, 1991.
5. **Boyle JT, Altschuler AM, Nixon TE, Tuchman DN, Pack AI, and Cohen S.** Role of the diaphragm in the genesis of lower esophageal sphincter pressure in the cat. *Gastroenterology* 88: 723–730, 1985.
6. **Clark MD, Rinaldo JA Jr, and Eyler WR.** Correlation of manometric and radiologic data from the esophagogastric area. *Radiology* 94: 261–270, 1970.
7. **DeMeester TR, Bonavani L, and Albertucci M.** Nissen fundoplication for gastroesophageal reflux disease. Evaluation of primary repair in 100 consecutive patients. *Ann Surg* 204: 9–20, 1986.
8. **Dodds WJ, Stewart ET, Hodges D, and Zboralske FF.** Movement of the feline esophagus associated with respiration and peristalsis. An evaluation using tantalum markers. *J Clin Invest* 52: 1–13, 1973.
9. **Dodds WJ, Hogan WJ, Stewart ET, Stef JJ, and Arndorfer RC.** Effects of increased intra-abdominal pressure on esophageal peristalsis. *J Appl Physiol* 37: 378–383, 1974.
10. **Dusey MP.** *Numerical Analysis of Lubrication Theory and Peristaltic Transport in the Esophagus* (PhD Thesis). University Park, PA: The Pennsylvania State Univ., 1993.
11. **Edmundowizc SA and Clouse RE.** Shortening of the esophagus in response to swallowing. *Am J Physiol Gastrointest Liver Physiol* 260: G512–G516, 1991.
12. **Gotley DC, Smithers BM, Menzies B, Branicki FJ, Rhodes M, and Nathanson L.** Laproscopic Nissen fundoplication and postoperative dysphagia–can it be predicted? *Ann Acad Med Singapore* 25: 646–649, 1996.
13. **Gregersen H, Lee TC, Chien S, Skalak R, and Fung YC.** Strain distribution in the layered wall of the esophagus. *J Biomech Eng* 121: 442–448, 1999.
14. **Hunter JG, Swanstrom L, and Waring JP.** Dysphagia after laparoscopic antireflux surgery. The impact of operative technique. *Ann Surg* 224: 51–57, 1996.
15. **Kadirkamanathan SS, Evans DF, and Swain CP.** The mechanical model of gastroesophageal reflux: what are the most important factors causing gastroesophageal reflux? In: *The Esophagogastric Junction 420 Questions–420 Answers*, edited by Giuli R, Galmiche JP, Jamieson GG, and Montrogue SC. Paris: John Libbey Eurotext, 1998, pp. 340–345.
16. **Kahrilas PJ, Lin S, Spiess AE, Brasseur JG, Joehl RJ, and Manka M.** Impact of fundoplication on bolus transit across esophagogastric junction. *Am J Physiol Gastrointest Liver Physiol* 275: G1386–G1393, 1998.
17. **Kahrilas PJ, Lin S, Chen J, and Manka M.** The effect of hiatus hernia on gastro-esophageal junction pressure. *Gut* 44: 476–482, 1999.
18. **Li M and Brasseur JG.** Nonsteady peristaltic transport in finite length tubes. *J Fluid Mech* 248: 129–151, 1992.
19. **Li M, Brasseur JG, and Dodds WJ.** Analyzes of normal and abnormal esophageal transport using computer simulations. *Am J Physiol Gastrointest Liver Physiol* 266: G525–G543, 1994.

20. **Li M, Brasseur JG, Kern MK, and Dodds WJ.** Viscosity measurements of barium-sulfate mixtures for use in motility studies of the pharynx and esophagus. *Dysphagia* 7: 17–30, 1992. (Reprinted by Brookfield Engineering Laboratories as publication no. AR-109, 1992).
21. **Lin S, Brasseur JG, Pouderoux P, and Kahrilas PJ.** The phrenic ampulla: distal esophagus or potential hiatal hernia? *Am J Physiol Gastrointest Liver Physiol* 268: G320–G327, 1995.
22. **Lundel L, Meyers JC, and Jamieson GG.** The effect of antireflux surgery on lower oesophageal sphincter tone and postprandial symptoms. *Scand J Gastroenterol* 28: 725–731, 1993.
23. **Mittal RK, Shaffer HA, Parollisi S, and Baggett L.** Influence of breathing pattern on the esophagogastric junction pressure and esophageal transit. *Am J Physiol Gastrointest Liver Physiol* 269: G577–G583, 1995.
24. **Nicosia MA.** *Muscle Mechanics and Modeling of the Esophagus During Swallowing* (PhD Thesis). University Park, PA: The Pennsylvania State Univ., 1997.
25. **Nicosia MA and Brasseur JG.** A Model for estimating muscle tension in vivo during esophageal bolus transport. *J Theor Biol* 219: 235–255, 2002.
26. **Nicosia MA, Brasseur JG, Liu JB, and Miller LS.** Longitudinal shortening in the human esophagus from high-frequency ultrasonography. *Am J Physiol Gastrointest Liver Physiol* 281: G1022–G1033, 2001.
27. **Pal A and Brasseur JG.** The mechanical advantage of local longitudinal shortening on peristaltic transport. *J Biomech Eng* 24: 94–100, 2002.
28. **Pandolfino JE, Shi G, Curry J, Joehl RJ, Brasseur JG, and Kahrilas PJ.** Esophagogastric junction distensibility: a factor contributing to sphincter incompetence. *Am J Physiol Gastrointest Liver Physiol* 282: G1052–G1058, 2002.
29. **Panton RL.** *Incompressible Flow*. New York: Wiley, 1996.
30. **Perdikis G, Hinder RA, Lund RJ, Raiser F, and Katada N.** Laparoscopic Nissen fundoplication: where do we stand? *Surg Laparosc Endosc* 7: 17–21, 1997.
31. **Pope CE.** Quality of life after anti-reflux surgery. *World J Surg* 16: 1147–1154, 1992.
32. **Ren J, Dodds WJ, Martin CJ, Dantas RO, Mittal R, Kern MK, and Brasseur JG.** Effect of increased intraabdominal pressure on peristalsis in the feline esophagus. *Am J Physiol Gastrointest Liver Physiol* 261: G417–G425, 1991.
33. **Ren J, Massey BT, Dodds WJ, Kern MK, Brasseur JG, Shaker R, Harrington WW, Hogan WJ, and Arndorfer TC.** Determinant of intrabolus pressure during esophageal peristaltic bolus transport. *Am J Physiol Gastrointest Liver Physiol* 264: G407–G413, 1993.
34. **Shi G, Pandolfino JE, Joehl RJ, Brasseur JG, and Kahrilas PJ.** Distinct patterns of oesphageal shortening during primary peristalsis, secondary peristalsis and transient lower oesophageal sphincter relaxations. *Neurogastroenterol Motil* 14: 505–512, 2002.
35. **Sloan S, Rademaker AW, and Kahrilas PJ.** Determinant of gastroesophageal junction incompetence: hiatal hernia, lower esophageal sphincter, or both? *Ann Intern Med* 117: 997–982, 1992.
36. **Tatum RP, Shi G, Manka MA, Brasseur JG, Joehl RJ, and Kahrilas PJ.** Bolus transit assessed by an esophageal stress test in postfundoplication dysphagia. *J Surg Res* 91: 56–60, 2000.
37. **Ulerich R, Dai Q, Miller LS, and Brasseur JG.** Detailed 3-D Anatomy of the Human Gastro-Esophageal Segment (Abstract). *Gastroenterology* 124, *Suppl*, S: A259, 2003.
38. **White FM.** *Fluid Mechanics*. New York: McGraw-Hill, 1999.